JOURNAL OF MATERIALS SCIENCE **39** (2004) 3031–3039

Dislocation structure in low-angle interfaces between bonded Si(001) wafers

T. AKATSU*, R. SCHOLZ, U. GÖSELE
Max-Planck-Institute of Microstructure Physics, Weinberg 2, 06120 Halle, Germany
E-mail: takeshi.akatsu@soitec.fr
E-mail: roscholz@mpi-halle.de
E-mail: goesele@mpi-halle.de

Dislocation structures of interfaces between bonded (001) Si wafers with co-existing low-angle twist and tilt misorientations were studied by transmission electron microscopy. At dominating twist, a square screw dislocation network accommodates the twist, and interacts with steps at the interface, forming 60-degree dislocations. As the step density, i.e., the tilt angle, increases relative to the twist angle, the density of so-called zigzag reactions increases. Finally, hexagonal dislocation meshes dominate the dislocation configuration. It was found that the plan-view observations give the crystallographic relations accurately. The structures of the dislocation configurations were analyzed using Bollmann's dualistic representation. The rotation axes and angles were determined.

1. Introduction

In recent years, wafer bonding (WB) techniques have rapidly been developed especially for semiconductor processes involved in the fabrication of silicon-on-insulator (SOI) wafers and micro-electrical-mechanical systems (MEMS). Direct wafer bonding of the same material without any intermediate layers has been shown to realize an atomically abrupt interface for the whole wafer area. However, even if the bonding aims at forming a perfect crystalline transition at the interface, in other words, re-forming a single crystal, some types of defects can be found in the bonding interface.

First, a small twist misalignment of the wafers of typically less than one degree is unavoidable even if undesired, and results in the formation of screw dislocation networks (SDN). In addition, a so-called miscut of the initial wafer surfaces induced during the wafer fabrication process incorporates an additional tilt misalignment. Depending on the ratio of twist to tilt misalignments, the dislocation arrangement may vary at the interface formed by a suitable bonding procedure and subsequent thermal treatments. The microstructure corresponds to a low angle grain boundary of mixed character. Usually the twist misalignment dominates, and can intentionally be increased by bonding wafers with a larger rotational misorientation.

Long before the process of large area wafer bonding was introduced, artificial grain boundaries in silicon (Si) with predominant rotation axes along [001] and [111] had been fabricated by sintering of single crystals and characterized by transmission electron microscopy (TEM) [1] and by electron diffraction [2]. Initial silicon WB experiments leading to the dislocation network formation in (001) interfaces were reported for so-called oxidewelded wafers [3], and for bonded hydrophobic wafer pairs [4, 5]. In these experiments, dislocation configurations were obtained after post-bonding heat treatments at 1100°C or 1200°C, to reach a high bond strength and/or to dissolve the interface oxide layer by diffusion. Detailed TEM investigations of Si wafers bonded in an ultra-high vacuum (UHV) at room temperature [6] and of hydrophobic wafer pairs treated at various temperatures [7] indicated the evolution of dislocation networks in WB interfaces at much lower temperatures. Recently a new bonding approach for preparing thousands of minute twist-type Si bicrystals in a single experiment was described [8].

The papers mentioned above showed not only the dislocation configurations at the bonding interfaces but also the existence of various preparation or bonding artefacts such as oxide and carbide precipitates and voids in the nanometer to sub-micron level. The most dominating feature of dislocation arrangement in Si (001) WB interfaces is a square network of screw dislocations accommodating the twist rotation around [001]. In addition, reactions of so-called 60-degree dislocations are introduced in the square network by a small tilt component due to surface steps.

The present paper describes the dislocation networks formed in WB interfaces by increasing the tilt portion relative to the twist portion. Plan-view TEM observations are analyzed by using Bollmann's dualistic representation [9]. Methods are proposed to calculate the total rotation axis and angle.

* *Present address*: SOITEC, Parc technologique des Fontaines, Bernin 38926, Crolles Cedex, France.

TABLE I Tilt axes and preparation conditions of the silicon wafer pairs investigated

Sample	Tilt axis	Preparation conditions
A	Parallel to ⟨110⟩	Bonded in UHV at RT, annealed at 1100°C
B	Parallel to ⟨110⟩	Amorphous surface bonded to hydrophobic surface, annealed at 1000°C
C	Parallel to ⟨110⟩	Hydrophobic surfaces bonded under cleanroom conditions, annealed at 700°C
D	Parallel to ⟨110⟩	Bonded in UHV at RT, annealed at 1100°C
E	Not parallel to ⟨110⟩	Hydrophobic surfaces bonded under cleanroom conditions, annealed at 700°C

TABLE II Measured dislocation spacings and calculated misorientation angles

Sample	L_s (nm)	L_t (nm)	θ_{twist} (deg)	θ_{tilt} (deg)
A	8.6–8.8	27–29	2.53 ± 0.03	0.56 ± 0.02
B	16–17	28–29	1.34 ± 0.06	0.53 ± 0.02
C	34–38	27–29	0.63 ± 0.02	0.55 ± 0.03
D	42–46	31–33	0.50 ± 0.02	0.49 ± 0.02

2. Experimental

Five bonded wafer pairs, described by the letters A–E, are considered in the present paper. These samples were chosen among many other samples that have been investigated so far by the authors. Samples A–D have the tilt axes almost parallel to a ⟨110⟩ direction (see Appendix A), while samples E does not. The samples originated from various bonding experiments, as follows: Samples A and D were bonded in UHV at room temperature (RT) followed by annealing at 1100°C. For samples C and E, hydrophobic Si surfaces were bonded under cleanroom conditions and annealed at 700°C. For sample B, an amorphous silicon wafer surface was bonded to a hydrophobic crystalline surface, followed by annealing at 1000°C. Thus, the amorphous Si layer recrystallized and bonding of crystalline Si occurred at the interface. The tilt axes and the preparation conditions of the different samples A–E are summarized in Table I.

For plan-view TEM investigations of bonding interfaces, the specimens were prepared first by cutting 25 degrees inclined to the interface plane, and by mechanical grinding, dimpling and Ar ion milling. The plan-view TEM was carried out by using a Phillips CM20T microscope at 200 kV. For measurements of misorientation angles, electron diffraction patterns were taken from plan-view samples as well as from cross section samples, that were additionally prepared very close to the plan-view specimens from each bonded wafer pair.

3. Results and discussions

3.1. Plan-view transmission electron microscopy

Bright field plan-view micrographs of the bond interfaces of samples A–E are shown in Fig. 1a–e, respectively. The micrographs were taken under multi-beam imaging conditions with the specimens tilted about 1 to 1.5 degrees away from the [001] zone axis that is almost normal to the bond interface. This gives the best contrast of the whole dislocation content and suppresses strong disturbing moiré contrasts. Selected weak beam dark field images of our interfaces as applied in the literature [2, 5] confirmed the main features of the dislocation structure.

In all the figures, the micrographs are cut so that the borders of the figures are almost parallel to ⟨110⟩ directions, i.e., parallel to screw dislocations. Both screw dislocation sets can be clearly recognized in Fig. 1a and e. On the other hand, in Fig. 1b, c, and d, one set of the screw dislocations are seen as horizontal dislocation segments. The other set of screw dislocations are observed as vertical lines forming four-fold nodes with the horizontal segments. In addition to these screw dislocation sets, another set of dislocations with a typical zigzag shape is present in the vertical direction in Fig. 1a–d. Since these dislocations correspond to the tilt mislignment of the wafer pairs, we call them "tilt" dislocations in the present paper. The tilt dislocations react with the horizontal screw dislocation segments, forming three-fold nodes, and cause a half-distance shift between the horizontal screw dislocation segments. Such zigzag lines and reactions in square screw dislocation networks are well-known elements of grain boundary structures [1, 10, 11]. In Fig. 1e, the tilt dislocations run inclined to the screw dislocations. The origin of the tilt dislocations may be attributed to the steps at the initial wafer surfaces mainly due to the miscut. It is considered that, at interface formation, by diffusion processes during the heat treatments, the initial surface step structures of both wafers are incorporated as a set of tilt dislocations with regular spacing. The mean spacing of each dislocation set was measured from the micrographs, as listed in Table II. L_s is the mean spacing of the screw dislocations perpendicular to the tilt dislocations, while L_t, is the mean spacing of the tilt dislocations.

In the sequence of Fig. 1a to d, the proportion of L_t to L_s decreases. Accordingly, the number of four-fold dislocation nodes of the screw dislocations, which is a characteristic of square networks, decreases. Consequently, more hexagonal dislocation meshes can be observed, characterized by three-fold dislocation nodes. Regular hexagonal meshes of screw dislocations are known as characteristic features of pure (111) twist boundaries. This means that, in our boundaries A to D, we observe obviously a mixture of dislocation arrangements typical for (001) and (111) twist boundaries. In the first four samples A–D, the tilt axes lie almost in a ⟨110⟩ direction in the interface, i.e., parallel to one set of the screw dislocations. Thus, one can presume the resulting rotation axis of these boundaries in directions lying between ⟨001⟩ and ⟨111⟩.

3.2. Determination of misorientation angles

The tilt and twist angles were measured and estimated by using two methods to confirm the obtained values. The first method is to calculate the angles from the spacing of the dislocations observed in plan-view TEM. The second method utilizes diffraction patterns. The first method needs only one plan-view TEM image, and is therefore convenient. On the other hand, the second

method gives the crystallographic relationships more directly using diffraction patterns.

The twist and tilt angles, θ_{twist} and θ_{tilt}, can be calculated from the spacing of the screw and tilt dislocations, L_s and L_t, as follows:

$$\theta_{\text{twist}} = \arcsin(a/\sqrt{2}L_s) \quad (1)$$

$$\approx a/\sqrt{2}L_s \quad (2)$$

$$\theta_{\text{tilt}} = \arctan(a/\sqrt{2}L_t) \quad (3)$$

$$\approx a/\sqrt{2}L_t. \quad (4)$$

Here it is assumed that all the tilt dislocations in each observation have the same line sense, and also that all the screw dislocations of the same set have the same line sense. This could be confirmed by the fact that the contrast change at each dislocation segment is the same. The calculated values are listed in Table II, with an error of less than 0.06°.

The tilt angles were additionally measured using Kikuchi lines in the diffraction patterns taken from the same plan-view TEM samples as that of Fig. 1. By reading the difference in the position of the same Kikuchi lines between the two crystals, R, the angle between the two crystals can be calculated as follows:

$$\theta = \arcsin(R/L) \approx R/L, \quad (5)$$

where L is the camera length of the microscope for each acquisition. Thus, the angles were measured with an error of less than 0.04° (Table III).

The twist angles were also obtained by measuring the rotation angle of the Kikuchi lines from the same plan-view TEM specimens. However, the accuracy was only 0.2°. Therefore, cross-section TEM specimens were

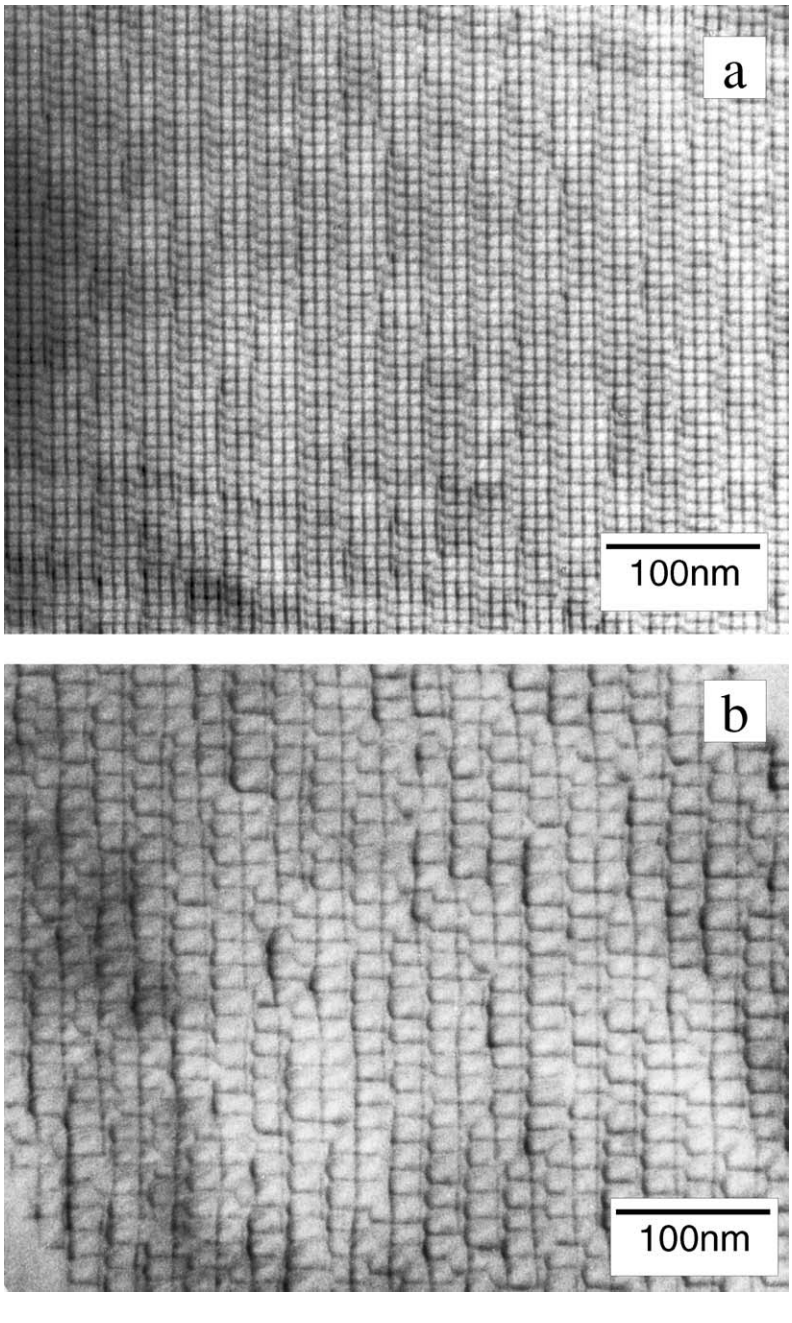

Figure 1 (a)–(e) Plan-view TEM images of the dislocation configurations in five different Si wafer bonding interfaces (samples A–E). (*Continued*)

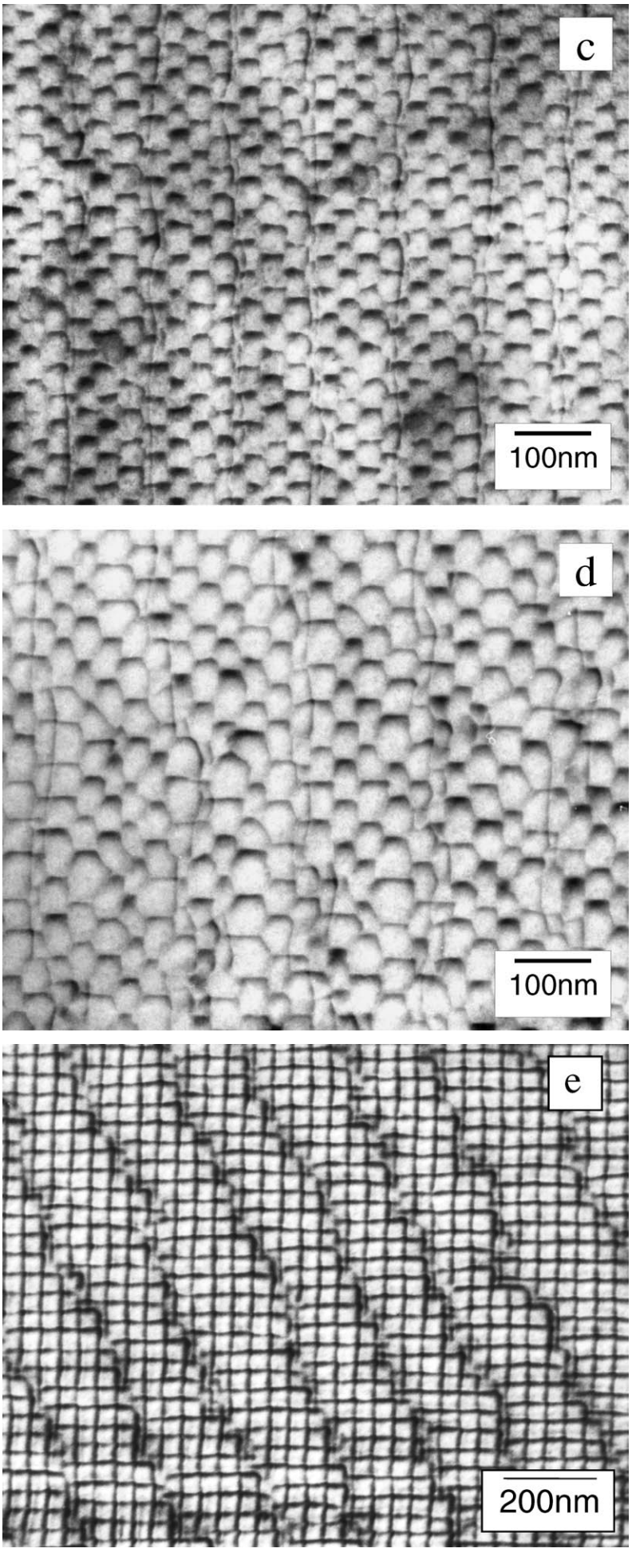

Figure 1 (*Continued*).

TABLE III Angles measured from the diffraction patterns; twist angles and tilt angles were measured from cross-section and plan-view samples, respectively

Sample	θ_{twist} (deg)	θ_{tilt} (deg)	θ_{total} (deg)
A	2.55 ± 0.05	0.54 ± 0.04	2.59 ± 0.03
B	1.34 ± 0.03	0.53 ± 0.04	1.44 ± 0.06
C	0.69 ± 0.02	0.53 ± 0.04	0.84 ± 0.03
D	0.53 ± 0.01	0.46 ± 0.03	0.70 ± 0.03

prepared from regions near the region of the plan-view sample of each bonded wafer pair. In this way, the twist angles were determined more accurately using Equation 5. The values obtained are shown in Table III. They agree well with those values that were calculated from the plan-view images. This also clearly indicates that all the tilt dislocations in each sample have the same sign. For sample C and D, a difference of up to 0.06° is seen, which may be attributed to a deviation of the wafer surface roughness. In other words, such a deviation might exist within a region of even a couple of millimeters, when two TEM samples are used.

These calculations clearly indicate that the first method using the spacing of the dislocations gives values as accurately as when diffraction patterns are used. The method using the spacing of the dislocations is more reliable, in that the twist and tilt angle of the region can be obtained from one single TEM plan-view sample. Moreover, it is more convenient since it needs only one TEM specimen, unlike the other method, which requries an additional cross-section specimen for a high accuracy in angle measurement. Therefore, in the following discussions, the values of the twist and tilt angles from the plan-view images (Table II) are used.

The total rotation angle can be expressed using the tilt and twist angles [12]:

$$\cos(\theta/2) = \cos(\theta_{tilt}/2)\cos(\theta_{twist}/2) \qquad (6)$$

The geometry of the interface and the expressions of the grain boundary are discussed in detail in the reference book. Therefore, we use the formula for the present paper. Using Equation 6, the total rotation angles for samples A–D can be obtained as shown in Table III.

3.3. Dualistic representation of the dislocation networks

Bollmann [9] introduced a method to analyze dislocation arrangements in grain boundaries. By applying this method, dislocation line configurations and the diagram of the corresponding Burgers vectors can be dualistically represented. It enables one to determine the rotation axis of the grain boundaries from the Burgers vector diagram. The dislocation lines and the corresponding Burgers vectors are considered separately and represented as L- and B-diagram. The B-diagram is drawn with periods equal to the periods of the L-diagram, and a two coordinate numbering is introduced.

First, we consider the simple case of one so-called foreign [9] or extraneous dislocation [11], which is in reaction with a square screw dislocation network located in a (001) plane. In Fig. 2, a foreign dislocation is introduced parallel to one of the two screw dislocation sets extending in ⟨110⟩ directions. It was found that such a foreign dislocation might cause a zigzag reaction as drawn in Fig. 2a. The corresponding B-diagram can be constructed as shown in Fig. 2b, by applying the dualistic relations.

To describe the reactions at the triple nodes, it is necessary that two different Burgers vectors of the type $a/2\ \langle 101 \rangle$ have the same component perpendicular to the (001) plane of the square network (Fig. 2b). The triangular polygons, which entail such Burgers vectors, lie on one of the two possible {111} planes (dashed area), i.e., either $(\bar{1}11)$ or $(\bar{1}1\bar{1})$ depending on the sense of the atomic step. This results in a step in the otherwise two-dimensional B-diagram of the pure twist boundary. The B-diagram in Fig. 2b is presented as the projection

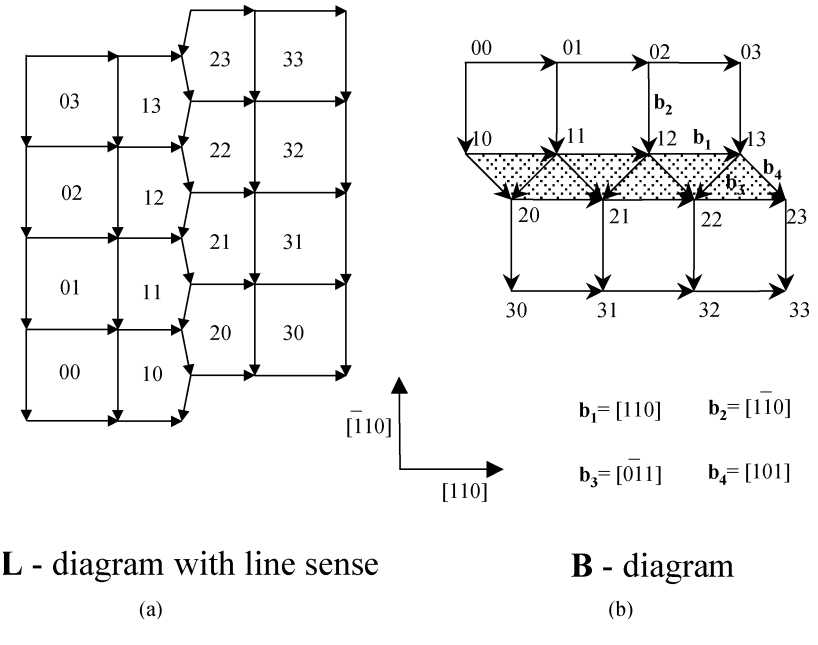

Figure 2 Dislocation line (L) diagram and Burgers vector (B) diagram of a screw dislocation network reacting with a tilt dislocation.

onto a (001) plane, a plane perpendicular to the rotation axis of the pure twist boundary. The step in the B-diagram, therefore, represents the introduction of a tilt component in the twist boundary. Fig. 2 shows one of the possible combinations of Burgers vectors. The B-diagram can be superimposed on the L-diagram by a rotation of 90 degrees. Then the numbered B-nodes coincide with the corresponding fields of the L-diagram, and the connections in the L-diagram can be followed from the B-diagram. The line sense of the dislocations is indicated by arrows, fulfilling the Burgers vector combinations at the reaction sites and the screw dislocation nodes (Fig. 2).

In a concrete case, not only the rotation axis and angle but also their signs such as the directions of twist and tilt rotation should be determined. For example, the sign of the {111} step, i.e., up or down from the interface plane, in the B-diagram depends on the sign of the atomic step at the interface. In fact, the sign of the tilt and twist direction between the two bonded crystals can easily be determined by electron diffraction patterns from outside the interface region using 25-degree cut specimens. In addition, the polarity of the sign does not affect the appearance of the dislocation configurations under discussion. Therefore, the real signs in our examples are not discussed in detail in this paper.

TABLE IV m (m*), n (n*), and ω (ω*) for samples A–D

Sample	m	(m*)	n	(n*)	ω	ω*
A	2–4	(2.9)	1		[1 1 7]	[1 1 6.80]
B	1–2	(1.22)	1		[1 1 3]	[1 1 3.44]
C	1		3–4	(3.33)	[3 3 5]	[1 1 1.60]
D	1		3–6	(4.7)	[5 5 7]	[1 1 1.43]

This discussion is now applied to samples A–D, which have tilt dislocations parallel to one of the screw dislocation sets. B-diagrams can be constructed so that they match the observed dislocation configuration. As discussed above, three-fold and four-fold nodes characterize the dislocation network. Accordingly, the periodicity of the dislocation configuration may be expressed by the number of four-fold nodes, m, and the number of three-fold nodes, n, per one periodicity in the $[\bar{1}10]$ direction in the B-diagram. The values of (m, n) obtained from the plan-view micrographs are listed in Table IV. It was found that (m, n) = (3, 1), (1, 1), (1, 3) and (1, 5) fit approximately the configurations of samples A to D, respectively. B-diagrams for those (m, n) are constructed in Fig. 3, again as projections on a (001) plane.

As long as the number of the screw dislocations between two tilt dislocations, m, is larger than one, the

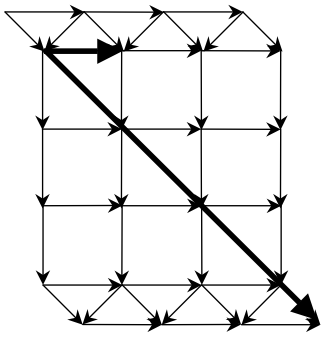

(m, n) = (3, 1)

$\boldsymbol{B}_1$ = [1 1 0], $\boldsymbol{B}_2$ = [7 0 1]

$\boldsymbol{\omega}$ = [$\boldsymbol{B}_1$ x $\boldsymbol{B}_2$] = [-1 1 7]

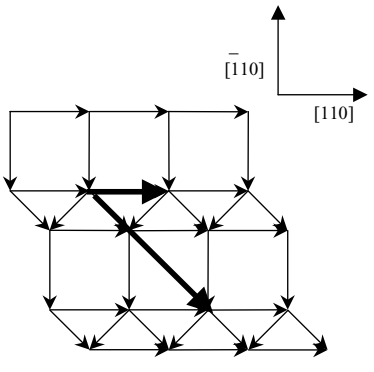

(m, n) = (1, 1)

$\boldsymbol{B}_1$ = [110], $\boldsymbol{B}_2$ = [3 0 1]

$\boldsymbol{\omega}$ = [$\boldsymbol{B}_1$ x $\boldsymbol{B}_2$] = [-1 1 3]

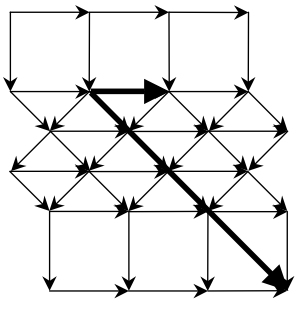

(m, n) = (1, 3)

$\boldsymbol{B}_1$ = [110], $\boldsymbol{B}_2$ = [5 0 3]

$\boldsymbol{\omega}$ = [$\boldsymbol{B}_1$ x $\boldsymbol{B}_2$] = [-3 3 5]

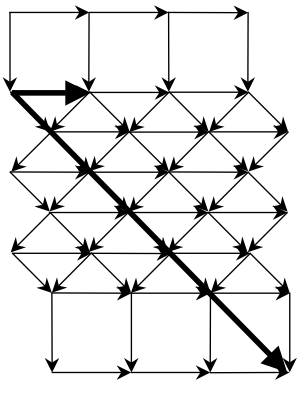

(m, n) = (1, 5)

$\boldsymbol{B}_1$ = [110], $\boldsymbol{B}_2$ = [7 0 5]

$\boldsymbol{\omega}$ = [$\boldsymbol{B}_1$ x $\boldsymbol{B}_2$] = [-5 5 7]

Figure 3 B-diagrams of dislocation configurations in Fig. 1a–d for different periodicities (m, n) = (3, 1), (1, 1), (1, 3) and (1, 5).

L-diagram consists of one tilt dislocation and m screw dislocations parallel to each other, and the other set of the screw dislocations perpendicular to the former two. This corresponds to the cases of samples A–B. If there exist more tilt dislocations than screw dislocations as for samples C–D, then the L-diagram consists of one screw dislocation and n tilt dislocations, and the other set of the screw dislocations perpendicular to the former two. Here in Fig. 3 only the corresponding B-diagrams are shown for simplicity. All the triangular B-polygons lie in reality on {111} planes and describe together with the square polygons on (001) a stepped B-diagram defining a mean plane perpendicular to the rotation axis of the respective grain boundary. The (111) sections contain Burgers vector combinations representative for ideal hexagonal dislocation networks with ⟨111⟩ rotation axis.

3.4. The total rotation axes acquired from the Burgers vector diagrams

From Frank's formula,

$$\boldsymbol{B}_{\mathrm{i}} = [\boldsymbol{\omega} \times \boldsymbol{r}_{\mathrm{i}}], \tag{7}$$

where $\boldsymbol{B}_{\mathbf{i}}$ is a transient vector in the B-space, $\boldsymbol{r}_{\mathbf{i}}$ is the corresponding vector in the crystal lattice, and $\boldsymbol{\omega}$ is the rotation axis. $\boldsymbol{B}_{\mathbf{i}}$ is perpendicular to $\boldsymbol{\omega}$. Therefore, the rotation axis $\boldsymbol{\omega}$ can be calculated as a vector product of two independent $\boldsymbol{B}_{\mathbf{i}}$ in each B-diagram, using

$$\boldsymbol{\omega} = [\boldsymbol{B}_{\mathrm{i}} \times \boldsymbol{B}_{\mathrm{j}}]. \tag{8}$$

Two $\boldsymbol{B}_{\mathbf{i}}$ vectors should be taken between two nodes in the B-diagram which describe its periodicity, as shown in Fig. 3. In the case of samples A to D, the tilt dislocations lie in a [110] direction. Accordingly, one translation vector can be taken as

$$\boldsymbol{B}_1 = [110]. \tag{9}$$

Another $\boldsymbol{B}$ vector can be chosen to be

$$\boldsymbol{B}_2(\mathrm{m}, \mathrm{n}) = [2\mathrm{m} + \mathrm{n}, 0, \mathrm{n}]. \tag{10}$$

Therefore, the total rotation axis $\boldsymbol{\omega}$ can be obtained as

$$\boldsymbol{\omega} = [\boldsymbol{B}_1 \times \boldsymbol{B}_2] = [-\mathrm{n}, \mathrm{n}, 2\mathrm{m} + \mathrm{n}]. \tag{11}$$

For the case of (m, n) = (3, 1),

$$\boldsymbol{B}_1 = [110], \boldsymbol{B}_2 = [7, 0, 1], \tag{12}$$

therefore,

$$\boldsymbol{\omega} = [\boldsymbol{B}_1 \times \boldsymbol{B}_2] = [-1, 1, 7]. \tag{13}$$

Likewise, $\boldsymbol{B}_2$ and $\boldsymbol{\omega} = [\boldsymbol{B}_1 \times \boldsymbol{B}_2]$ were obtained for the other three combinations as shown in Fig. 3.

The B-diagrams in Fig. 3 describe only approximately the real dislocation arrangements for discrete (m, n) states. In reality, by close inspection of the images in Fig. 1a to d several (m, n) states can be recognized as given in Table IV. As a result, mean values of m and n, m^* and n^*, are usually not integers. For such cases, the total rotation axis can be obtained by substituting (m^*, n^*) for (m, n) in Equations 10 and 11:

$$\boldsymbol{B}_2^*(\mathrm{m}^*, \mathrm{n}^*) = [2\mathrm{m}^* + \mathrm{n}^*, 0, \mathrm{n}^*]. \tag{14}$$

$$\boldsymbol{\omega}^* = [\boldsymbol{B}_1 \times \boldsymbol{B}_2^*] = [-\mathrm{n}^*, \mathrm{n}^*, 2\mathrm{m}^* + \mathrm{n}^*]. \tag{15}$$

For sample D, as an example, $(\mathrm{m}^*, \mathrm{n}^*) = (1, 4.7)$, giving:

$$\boldsymbol{\omega}^* = [\boldsymbol{B}_1 \times \boldsymbol{B}_2^*] = [-4.7, 4.7, 6.7] = [-1, 1, 1.43] \tag{16}$$

Similarly, the rotation axes of the other cases were calculated and listed in Table IV.

3.5. Application to a more general dislocation network structure

Fig. 1e shows the plan-view TEM image of sample E, where the tilt axis does not lie in a ⟨110⟩ direction. A corresponding B-diagram can be constructed, which represents the dislocation configuration observed (Fig. 4). Two independent translation vectors should be found marked with arrows in Fig. 4 as $\boldsymbol{B}_1$ and $\boldsymbol{B}_2$:

$$\boldsymbol{B}_1 = [4, 10, 0] \tag{17}$$

$$\boldsymbol{B}_2 = [9, 6, 1] \tag{18}$$

$$\boldsymbol{\omega} = [\boldsymbol{B}_1 \times \boldsymbol{B}_2] = [-5, 2, 33]. \tag{19}$$

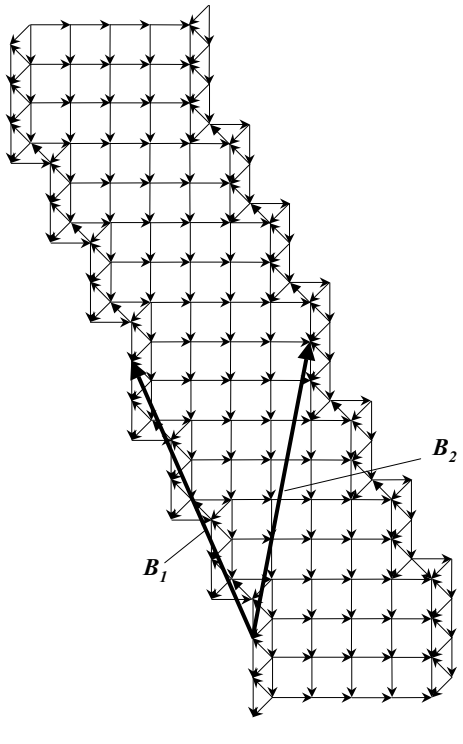

Figure 4 B-diagram of a representative section of the dislocation network in sample E (Fig. 1c).

TABLE V Rotation axis ω and the twist, tilt and total rotation angles for sample E

Sample	ω	θ_{twist} (deg)	θ_{tilt} (deg)	θ_{total} (deg)
E	[−5, 2, 33]	0.539	0.083	0.55

In this case, the $\boldsymbol{B}_1$ and $\boldsymbol{B}_2$ are both high index vectors, representing the mean periodicity of the B-diagram. Therefore, the consideration for finding the (m^*, n^*), which we have done for samples A–D, is not necessary.

The mean spacing of the screw dislocation network, L_s, and that of the tilt dislocation, L_t, can be measured from Fig. 1e: $L_s = 40.8$ nm and $L_t = 187.5$ nm, respectively. Therefore, the twist and tilt angles can be obtained by using Equations 1 and 3, $\theta_{\text{twist}} = 0.54^\circ$, $\theta_{\text{tilt}} = 0.08^\circ$. Accordingly, the total rotation angle is calculated by using Equation 6: $\boldsymbol{\theta}_{\text{total}} = 0.55^\circ$. These values are summarized in Table V.

5. Conclusions

The configurations of dislocations were studied at (001) Si wafer bonded interfaces with co-existing low-angle tilt and twist misalignments. A two-dimensional square screw dislocation network does no longer dominate the interface structure when the tilt angle is close to the twist angle, independent of the degree of the misalignment. The arrangement of the dislocations was quantitatively described by Bollmann's dualistic representation. It was shown that the plan-view TEM observation alone can allow to determine the geometrical relationship at the interface between the bonded wafer pairs.

Acknowledgements

The authors thank A. Plößl and Q.-Y. Tong for bonded samples, and S. Hopfe for the TEM sample preparation. We also thank M. Reiche for discussions on Si wafers and U. Messerschmidt for careful reading of the manuscript.

Appendix A

The tilt dislocations lying in a ⟨110⟩ direction are often observed, and are therefore not rare cases in wafer bonding. The reason is discussed in this appendix.

It can be considered that main reasons to cause the misorientation of the wafer surface orientation lie in the wafer cutting process. Bowing and tapering of the wafer surface can also cause misorientation even on one wafer surface. However, the misorientation of the cutting blade to the crystal orientation should lead to a misorientation, or miscut, of the whole wafer surface to the same extent for all the wafers that are cut from the same single crystal ingot. This misorientation, or miscut, causes surface steps on the wafer surface. The rotation axis of this miscut to the ideal (001) plane, ω, lies in the direction of the surface steps (Fig. A1).

Often, the wafer bonding is done by combining two wafers A and B, originating from the same ingot by the same series of the cutting process. Now, one of water (B) is flipped over around the $[1\bar{1}0]$ axis and bonded to the other one (A) by aligning the major flats. The rotation axis of the flipped wafer is now transformed to $\omega_b'(= -\omega_b)$ to the coordination of the crystal of wafer A. At the bonded interface, the resulting rotation axis is $\omega = \omega_a + \omega_b' = [\bar{1}10]$. The spacing of the resulting tilt dislocations at the interface depends on the miscut angle and the direction of $\omega_a(= \omega_b)$.

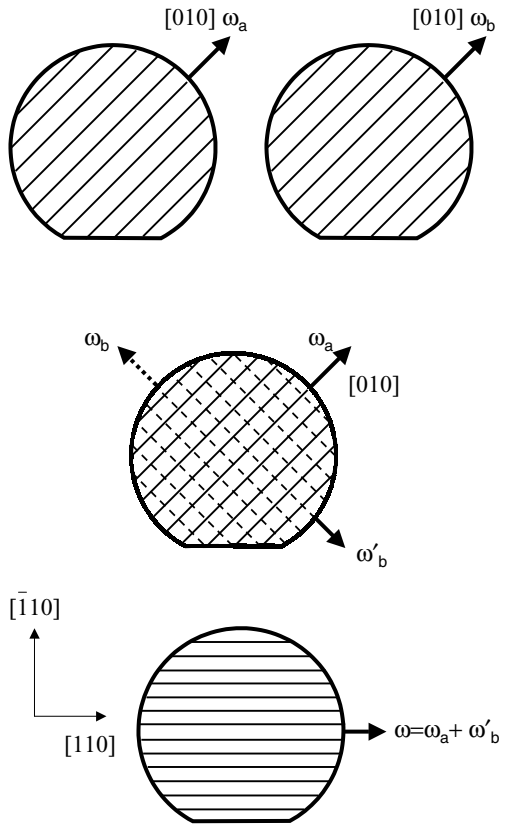

Figure A1 Schematic of a pair of wafers to bond, which results in the tilt dislocations parallel to one of the ⟨110⟩ directions.

References

1. H. FÖLL and D. AST, *Phil. Mag.* A **40** (1979) 589.
2. C. B. CARTER, H. FÖLL, D. AST and S. L. SASS, *ibid.* A **43** (1981) 441.
3. G. C. PERREAULT, S. L. HYLAND and D. G. AST, *ibid.* A **64** (1991) 64.
4. R. GAFITEANU, S. CHEVACHAROENKUL, U. M. GÖSELE and T. Y. TAN, in "Microscopy of Semiconducting Materials 1993," Inst. Phys. Conf. Ser. No. 134, edited by A. Cullis, A. E. Staton-Bevan and J. L. Hutchinson (Inst. Phys. Publ., Bristol, 1993) p. 87.
5. M. BENAMARA, A. ROCHER, A. LAPORTE, G. SARRABAYROUSE, L. LESCOUZERES, A. PEYRELAVIGNE, M. FNAIECH and A. CLAVERIE, *Mater. Res. Soc. Symp. Proc.* **378** (1995) 863.
6. A. PLÖSSL, R. SCHOLZ and T. AKATSU, in "Semiconductor Wafer Bonding: Science, Technology, and Applications V," Electrochemical Society Proceedings, Vol. 99–35, edited by C. E. Hunt, H. Baumgart, U. Gösele and T. Abe (Pennington, New Jersey, The Electrochem. Soc., 2001) p. 232.
7. R. SCHOLZ, L. F. GILLES, S. HOPFE, A. PLÖSSL and U. GÖSELE, in "Microscopy of Semiconducting Materials 1999," Inst. Phys. Conf. Ser. No. 164, edited by A. Cullis and R. Beanland (Inst. Phys. Publ., Bristol, 1999) p. 439.

8. C. CHEN, K. N. TU, C. H.TUNG, T. T. SHENG, A. PLÖSSL, R. SCHOLZ and U. GÖSELE, *Phil. Mag.* A **80** (2000) 881.
9. W. BOLLMANN, *ibid.* A **7** (1962) 1513.
10. S. AMELINCKX and W. DEKEYSER, in "Solid State Physics," Vol. 8, edited by F. Seitz and D. Turnbull (Academic Press, New York, 1959) p. 325.
11. T. SCHOBER and R. W. BALLUFFI, *Phil. Mag.* **24** (1971) 165.
12. P. SUTTON and R. W. BALLUFFI, in "Interfaces in Crystalline Materials" (Clarendon Press, Oxford, 1995) p. 23.

Received 26 June
and accepted 30 December 2003